SUPPLEMENTARY MATERIAL

Dissecting functional cooperation among protein subunits in archaeal RNase P, a catalytic ribonucleoprotein complex

Wen-Yi Chen[1,2,3], Dileep K. Pulukkunat[1,3,4], I-Ming Cho[1,3,5], Hsin-Yue Tsai[1,2,3] and Venkat Gopalan[1,2,3,4,5,*]

Department of Biochemistry[1]

Molecular Cellular Developmental Biology Program[2]

Center for RNA Biology[3]

Ohio State Biochemistry Program[4]

Department of Molecular Genetics[5]

The Ohio State University, Columbus, OH 43210, USA

The authors wish it to be known that, in their opinion, the first two authors should be regarded as joint First Authors.

* To whom correspondence should be addressed. Tel: +1 614-292-1332; Fax: +1 614-292-6773; Email: gopalan.5@osu.edu

Present addresses:

Dileep K. Pulukkunat, Department of Chemistry, Columbia University, New York, NY

Hsin-Yue Tsai, Program in Molecular Medicine, University of Massachusetts Medical School, Worcester, MA

MATERIALS AND METHODS

Abbreviations. *Eco*, *Escherichia coli*; *Mja*, *Methanocaldococcus jannaschii*; *Mth*, *Methanothermobacter thermautotrophicus*; *Pfu*, *Pyrococcus furiosus*; pre-tRNA, precursor tRNA; RPR, RNase P RNA; RPP, RNase P protein

Cloning of *Mja* RPRΔS and *Mja* RPRΔS Min. The gene encoding *Mja* RPRΔS was generated using a PCR-based deletion mutagenesis approach with pBT7-*Mja* RPR (1) as the template. Briefly, T4 polynucleotide kinase was used to phosphorylate the primers Mja RPRΔS-F and Mja RPRΔS-R (Table S1); these primers flank the region to be deleted and are oriented outward to ensure amplification of the entire plasmid without the nucleotides 67-192 in the *Mja* RPR-coding region. The resulting PCR products were circularized by ligation to generate pBT7-*Mja* RPRΔS, in which the ΔS derivative is controlled by a T7 RNA polymerase promoter.

A two-step PCR-based approach was adopted to generate a clone encoding *Mja* RPRΔS Min. Using pBT7-*Mja* RPRΔS as the template and Mja RPRΔS Min-F2 and Mja RPRΔS Min-R as primers, we first generated a 97-bp product containing the coding sequence corresponding to nts 26 to 112 of *Mja* RPRΔS Min. Using this 97-bp product as a template and Mja RPRΔS Min-F1 and Mja RPRΔS Min-R as primers, we then generated a 121-bp product

containing the entire coding sequence for *Mja* RPRΔS Min. This PCR product was digested with *Bam*HI, whose recognition site was included in Mja RPRΔS Min-R, and then cloned into pBT7 (2) that had been digested with *Stu*I (which generates a blunt end) and *Bam*HI. The resulting plasmid, pBT7-*Mja* RPRΔS Min, has the *Mja* RPRΔS Min gene under the control of a T7 RNA polymerase promoter.

Cloning of *Reclinomonas americana* mitochondrial (*Ram* mt) RPR. The gene encoding *Ram* mt RPR was amplified by PCR with the primers Ram mt RPR-F and Ram mt RPR-R, using as template a plasmid containing the *Ram* mt RPR gene (kind gift from Drs. Elias Seif and Franz Lang, University of Montreal, Canada) (3). The PCR product was digested with *Eco*RI, whose recognition site was included in the reverse primer, and then cloned into pBT7 (2) that had been digested with *Stu*I and *Eco*RI. The resulting plasmid, pBT7-*Ram* mt RPR, has the *Ram* mt RPR gene under the control of a T7 RNA polymerase promoter.

***In vitro* transcription of various RPRs used in this study.** Preparation of *Afu*, *Eco*, *Mja*, *Mth* and *Pfu* RPRs are described elsewhere (1,4,5). *Mja* RPR mutant derivatives were generated using the corresponding *Bsm*AI-linearized pBT7 plasmids as the template DNA for T7 RNA polymerase-mediated run-off transcription (6). For *Ram* mt RPR, the template was *Eco*RI-

linearized pBT7-*Ram*-mt RPR. The RNA transcripts thus generated were subsequently subjected to extensive dialysis to remove unincorporated rNTPs and their concentrations determined from Abs_{260} measurements and their respective extinction coefficients.

Cloning the genes encoding the archaeal RPPs. The genes encoding *Mth or Mja* POP5, RPP21, RPP29 and RPP30 (Table S2) were amplified by PCR from the respective genomic DNA using the corresponding gene-specific primers listed in Table S1. All PCR products were digested with *Bam*HI, whose recognition site was included in the various reverse primers. The *Mth*/*Mja* POP5- and RPP29-encoding ORFs were cloned into pLANT-2b (7) that had been digested with *Nde*I, filled in with Klenow, and subsequently digested with *Bam*HI. The *Mth*/*Mja* RPP21- and RPP30-encoding ORFs were cloned into pET-15b that had been digested with *Nco*I, filled in with Klenow, and subsequently digested with *Bam*HI. These cloning approaches ensured that no additional amino acid residues were introduced in the four encoded proteins.

Automated DNA sequencing at the OSU Plant-Microbe Genomics Facility was used to ascertain the sequence of the clones obtained using the procedures described above.

Construction of expression plasmids containing two archaeal RPP genes in tandem.

Mja RPPTC1: Digestion of pET-15b-*Mja*RPP30 with *Bgl*II and *Blp*I released the *Mja* RPP30 ORF together with its upstream T7 RNA polymerase promoter and downstream T7 terminator. This fragment was then inserted into pLANT-2b-*Mja* POP5 that had been digested with *Bam*HI and *Blp*I to generate *Mja* RPPTC1, a construct in which *Mja* POP5 and RPP30 are present in tandem, each with its own T7 RNA polymerase promoter and control elements as originally conceived in the pET system (8).

Mja RPPTC2: Digestion of pLANT-2b-*Mja* RPP29 with *Bgl*II and *Eco*RI released the *Mja*RPP29 ORF together with its upstream T7 RNA polymerase promoter and downstream T7 terminator as well as the RIL tRNA gene cluster present in pLANT-2b. This fragment was inserted into pET-15b-*Mja* RPP21 that had been digested with *Bgl*II and *Eco*RI to generate *Mja* RPPTC2, a construct in which *Mja* RPP21 and RPP29 are present in tandem.

Mth RPPTC1: The same approach as *Mja* RPPTC1 was used (except with *Mth* RPP-encoding plasmids) to generate a construct in which *Mth* POP5 and RPP30 are present in tandem.

Mth RPPTC2: Digestion of pET-15b-*Mth* RPP21 with *Bgl*II and *Blp*I released the *Mth* RPP21 ORF together with its upstream T7 RNA polymerase promoter and downstream T7 terminator. This fragment was inserted into pLANT-2b-*Mth* RPP29 that had been digested with *Bam*HI and *Blp*I to generate *Mth* RPPTC2, a construct in which *Mth* RPP21 and RPP29 are present in tandem.

Pfu RPPTC1: Digestion of pET-33b-*Pfu* RPP30 (5) with *Bgl*II, followed by fill-in with Klenow and digestion with *Blp*I released the *Pfu* RPP30 ORF with its upstream T7 RNA polymerase promoter and downstream T7 terminator. This fragment was inserted into pET-33b-*Pfu* POP5 (5) that had been digested with *Eco*RI, filled in with Klenow, and then digested with *Blp*I, to generate *Pfu* RPPTC1, a construct in which *Pfu* POP5 and RPP30 are present in tandem.

Pfu RPPTC2: Same approach as *Pfu* RPPTC1, except that the insert was derived from digestion of pET-33b-*Pfu* RPP21 and the vector recipient was pET-33b-*Pfu* RPP29. *Pfu* RPPTC2 is a construct in which *Pfu* RPP29 and RPP21 are present in tandem.

Overexpression of archaeal RPPs. For co-overexpression of archaeal binary RPPs in *E. coli* BL21(DE3) cells, we used plasmids in which the two ORFs were present in tandem. The

induction procedures were identical for *Mja*, *Mth* and *Pfu* RPPs. We use the *Mja* RPPs as a representative in the following description. *E. coli* BL21(DE3) cells were freshly transformed with pLANT-2b-*Mja* RPPTC1 or pET-15b-*Mja* RPPTC2. A single colony was used to inoculate 5 ml LB medium containing 35 µg/mL kanamycin (*Mja* POP5●RPP30) or 100 µg/mL carbenicillin (*Mja* RPP21●RPP29), respectively, and grown overnight at 37°C with shaking. These overnight cultures were used to inoculate 500 ml of fresh LB media containing the appropriate antibiotics. The cells were grown at 37°C with shaking and induced with 1 mM isopropyl-β-D-thio-galactoside (IPTG) at Abs_{600} ~0.6 to 0.8. To the RPP21●RPP29-expressing cultures, 1 mM $ZnCl_2$ was also added at the time of induction since RPP21 requires Zn^{2+} to fold properly (9,10). Subsequent to IPTG addition, the cells were were grown either at 37°C for 3 h (*Mja* RPP21●RPP29) or at 24°C for 15 h (*Mja* POP5●RPP30) and harvested by centrifugation. The cell pellets were stored at -80°C until further use.

Purification of archaeal binary RPP complexes.

Mja RPPs: Frozen cells (from a 125 ml culture) were thawed on ice and re-suspended in 20 ml of buffer A [25 mM Tris-HCl (pH 7.5), 5 mM DTT, 0.1 mM PMSF, 25 mM NaCl]. Subsequently, 5 ml of buffer S [25 mM Tris-HCl (pH 7.5), 5 mM DTT, 0.1 mM PMSF and 5 M NaCl] was added and the cells were lysed by sonication. Cell debris was pelleted by centrifugation (9,000 g, 15

min, 4°C). Polyethylenimine (PEI) was added to the cleared supernatant to a final concentration of 0.05% (v/v) and incubated on ice for 30 min. The PEI-precipitated nucleic acid was pelleted by centrifugation (9,000 g, 15 min, 4°C). To the resulting soluble fraction, finely powdered $(NH_4)_2SO_4$ was added slowly (to a final saturation of 40%) and precipitation performed over a period of 60 min with constant stirring on ice. The precipitated RPPs were recovered by centrifugation (9,000 g, 15 min, 4°C). The precipitate was dissolved in 3 ml of buffer RS [1 M $(NH_4)_2SO_4$, 25 mM Tris-HCl (pH 7.5), 5 mM DTT, 0.1mM PMSF, 25 mM NaCl] and diluted by adding buffer A to ensure a final $(NH_4)_2SO_4$ concentration of 375 mM. The solution was filtered through a 0.4 μm filter and loaded on a pre-equilibrated SP-Sepharose (GE Healthcare) column. The bound proteins were eluted with a 0 - 2 M NaCl gradient in buffer A. Binary complexes typically eluted between 1.2 and 1.5 M NaCl.

Mth RPPs: The purification procedures for *Mth* binary complexes were the same as *Mja* RPPs except that the final $(NH_4)_2SO_4$ concentration was adjusted to 250 mM before loading on SP-Sepharose. The binary complexes typically eluted at ~1.5 M NaCl.

Pfu RPPs: The purification procedures for *Pfu* binary proteins were the same as *Mja* RPPs except that *Pfu* POP5●RPP30 was precipitated with 80% $(NH_4)_2SO_4$ and the final $(NH_4)_2SO_4$

concentration was adjusted to either 175 mM (RPP21●RPP29) or 250 mM (POP5●RPP30) before loading on SP-Sepharose. The binary complexes typically eluted at ~1.5 M NaCl.

Other comments: An ÄKTA FPLC purifier (GE Healthcare) was used for all chromatographic procedures. Fractions containing the archaeal RPPs were identified by SDS-PAGE analysis and Coomassie Brilliant blue staining. Using the extinction coefficients of the binary RPP complexes and their Abs_{280} values, the concentration of each binary complex was calculated. The purified RPP complexes were dialyzed against 50 mM Tris-acetate (pH 8), 800 mM NH_4OAc and 10 mM $Mg(OAc)_2$, and stored at room temperature until further use.

Estimation of the molar ratio of *Pfu* POP5●RPP30 and RPP21●RPP29 binary complexes. About 2.5 μg of each RPP pair was separated in a 15% (w/v) acrylamide gel (37.5:1) using Tricine-SDS-PAGE (11) and stained with SYPRO Ruby protein gel staining dye (Invitrogen). The gels were imaged with VersaDoc System, which utilizes a CCD camera to capture UV-fluorescence images of the gels. The intensities of bands were analyzed using the software PDQuest (Bio-Rad). The relative stoichiometries were calculated from the intensities of the individual RPP bands and the molecular weight of the different RPPs.

Pulse-chase experiments with *Mth* RNase P to demonstrate that the dissociation rate (k_{-1}) is greater than the rate of chemical cleavage (k_2) under single-turnover conditions. These pulse-chase experiments were performed essentially as described elsewhere for studies on the hammerhead ribozyme (12). RPR folding, RNP assembly and assay conditions are elaborated in Materials & Methods (of the main text). *Mth* RPR (16.6 μM) was mixed with a trace amount of internally labeled pre-$tRNA^{Tyr}$ (~2 nM) and incubated at 55°C in a final reaction volume of 20 μl. From this mixture, two 5-μl aliquots were diluted 100-fold in 55°C pre-warmed assay buffer [50 mM MES (pH 5.8), 2 M NH_4OAc, 500 mM $MgCl_2$], one at 20 and the other at 30 min after the initiation of the reaction; the remainder proceeded without any dilution. Similarly, for *Mth* RPR + RPP21•RPP29 (3 μM), two 5-μl aliquots were diluted 100-fold in pre-warmed assay buffer [50 mM MES (pH 5.8), 800 mM NH_4OAc, 120 mM $MgCl_2$], one at 5 and the other at 10 min after the initiation of the reaction. From both the undiluted and diluted reactions, aliquots were removed at defined time intervals to measure the product formed. Reactions were terminated by adding stop solution [10 M urea, 5 mM EDTA, 0.05% (w/v) bromophenol blue, 0.05% (w/v) xylene cyanol, 10% (v/v) phenol]. The reaction products were separated on denaturing PAGE and quantitated as described in the Materials & Methods (of the main text).

REFERENCES

1. Pulukkunat, D.K. and Gopalan, V. (2008) Studies on *Methanocaldococcus jannaschii* RNase P reveal insights into the roles of RNA and protein cofactors in RNase P catalysis. *Nucleic Acids Res*, **36**, 4172-4180.

2. Tsai, H.Y., Lai, L.B. and Gopalan, V. (2002) A Modified pBluescript-based vector for facile cloning and transcription of RNAs. *Anal Biochem*, **303**, 214-217.

3. Seif, E., Cadieux, A. and Lang, B.F. (2006) Hybrid E. coli--Mitochondrial ribonuclease P RNAs are catalytically active. *RNA*, **12**, 1661-1670.

4. Boomershine, W.P., Raj, M.L., Gopalan, V. and Foster, M.P. (2003) Preparation of uniformly labeled NMR samples in *Escherichia coli* under the tight control of the araBAD promoter: expression of an archaeal homolog of the RNase P Rpp29 protein. *Protein Expr Purif*, **28**, 246-251.

5. Tsai, H.Y., Pulukkunat, D.K., Woznick, W.K. and Gopalan, V. (2006) Functional reconstitution and characterization of *Pyrococcus furiosus* RNase P. *Proc Natl Acad Sci USA*, **103**, 16147-16152.

6. Vioque, A., Arnez, J. and Altman, S. (1988) Protein-RNA interactions in the RNase P holoenzyme from *Escherichia coli*. *J Mol Biol*, **202**, 835-848.

7. Finkelstein, J., Antony, E., Hingorani, M.M. and O'Donnell, M. (2003) Overproduction and analysis of eukaryotic multiprotein complexes in *Escherichia coli* using a dual-vector strategy. *Anal Biochem*, **319**, 78-87.

8. Studier, F.W., Rosenberg, A.H., Dunn, J.J. and Dubendorff, J.W. (1990) Use of T7 RNA polymerase to direct expression of cloned genes. *Methods Enzymol*, **185**, 60-89.

9. Amero, C.D., Boomershine, W.P., Xu, Y. and Foster, M. (2008) Solution structure of *Pyrococcus furiosus* RPP21, a component of the archaeal RNase P holoenzyme, and interactions with its RPP29 protein partner. *Biochemistry*, **47**, 11704-11710.

10. Kakuta, Y., Ishimatsu, I., Numata, T., Kimura, K., Yao, M., Tanaka, I. and Kimura, M. (2005) Crystal structure of a ribonuclease P protein Ph1601p from *Pyrococcus horikoshii* OT3: an archaeal homologue of human nuclear ribonuclease P protein Rpp21. *Biochemistry*, **44**, 12086-12093.

11. Schagger, H. (2006) Tricine-SDS-PAGE. *Nature Protocols*, **1**, 16-22.

12. Stage-Zimmermann, T.K. and Uhlenbeck, O.C. (1998) Hammerhead ribozyme kinetics. *RNA*, **4**, 875-889.

13. Massire, C., Jaeger, L. and Westhof, E. (1998) Derivation of the three-dimensional architecture of bacterial ribonuclease P RNAs from comparative sequence analysis. *J Mol Biol*, **279**, 773-793.

Table S1

Oligonucleotides used in this study

Mja RPRΔS-F	GGGTGCAAGCCGGTTTC
Mja RPRΔS-R	ATAAATGGGGTGGGCGGAAC
Mja RPRΔS Min-F1	GGGCTGGTGACTTTCCGAAAGGAGGAAGTTCCGCCCACCC
Mja RPRΔS Min-F2	GGAAGTTCCGCCCACCCATAGGGTGCAAGCCGGTTTC
Mja RPRΔS Min-R	GCGGATCCCGGGGGCTATAGCCCGC
Ram mt RPR-F	ATAAAAGTTTATTGGATGTCTGATTATAATATATAATAGG
Ram mt RPR-R	GC*GAATTC*TTTAAAGTTTATTTATAAGCTGGATTTTGTCC
Mja POP5-F	TGATAGAAATGCTGAAAACACTGCCACCAACTTTAAGGG
Mja POP5-R	GG*GGATCC*TTATTTTTGTTTTTTAGCTTTCAACCTTTCTC
Mja RPP21-F	AAAAAGTTCTTAGAAAAAAGCTAAAGAAGATAGC
Mja RPP21-R	GG*GGATCC*TTAAGAGGTTTGTGAGTTTGATTTTGCTTTTAATCTTTCC
Mja RPP29-F	TGATCACTCCGCACAATATCCTGAGGCATGAACTTATAGGGC
Mja RPP29-R	GG*GGATCC*TAATACGGATACAGTATCTTTATTTTTTTCTTTAATCTC
Mja RPP30-F	CGTATCGATATCAACAGAATAGAAAAGGAAGAGG
Mja RPP30-R	GG*GGATCC*TCATTCTTTTTCTTCTTTTATAATTTCCACTCC
Mth POP5-F	TGAAGATCCTGCCACCAACACTGAGGGTCCCCAGG
Mth POP5-R	GC*GGATCC*TCAGTATTTATCTTTCTTGGAAGG
Mth RPP21-F	CGTCGTGGTAAGCGTCCACGTTGGATGTTAAAAATTGCTG
Mth RPP21-R	GC*GGATCC*TAACGGTCGCTCTGGCTTTCACCACATTTATTGTG
Mth RPP29-F	TGATCACCCCGCGTAATATTTTCAGGCATGAGCTTATTGG
Mth RPP29-R	GC*GGATCC*TACCATTTACGAAATTTCTTCTTTATTCTCTCCTC
Mth RPP30-F	ATTCCGCAACGTATTCTGATGAAATTCTTTGACTTCC
Mth RPP30-R	GC*GGATCC*TTAGCTCTCAGGCAGCAGCCTCACACCCTCTGC

Note: All oligonucleotides were purchased from either Integrated DNA Technologies or Sigma Genosys. Sequences are listed from 5′ to 3′. Restriction sites, if incorporated into primers to facilitate subsequent cloning into appropriate vectors, are shown in italic font.

Table S2

Characteristics of RPPs from different archaea

Organism	RPP	Gene ID	Isoelectric point (pI)	Predicted mass, Da
Pfu	POP5	PF1378	10.7	13,839
	RPP21	PF1613	11.0	14,271
	RPP29	PF1816	10.8	14,953
	RPP30	PF1914	10.3	24,494
Mth	POP5	MTH687	10.5	14,568
	RPP21	MTH1618	11.1	16,936
	RPP29	MTH11	11.4	10,722
	RPP30	MTH688	8.2	27,662
Mja	POP5	MJ0494	10.0	15,941
	RPP21	MJ0962	10.6	15,567
	RPP29	MJ0464	9.7	10,888
	RPP30	MJ1139	9.1	27,345

Note: Gene IDs and sequences from the Comprehensive Microbial Resource, J. Craig Venter Institute (http://cmr.jcvi.org).

Table S3

Quantitation of the stoichiometric ratio of *Pfu* RPPs in purified binary complexes*

Binary complex tested	Ratio
POP5•RPP30	1.1 ± 0.4**
RPP21•RPP29	0.9 ± 0.1**

* The values reported are the mean from at least two independent experiments.

** The numbers indicate the molecular ratio of POP5 to RPP30 and RPP21 to RPP29.

Table S4

Steady-state kinetic parameters for processing of *Eco* pre-tRNA^{Tyr} by *in vitro* reconstituted *Pfu* RNase P*

Type of *Pfu* RNase P reconstituted	k_{cat}, min^{-1}	K_M, μM
Pfu RPR + RPP21 + RPP29 + POP5 + RPP30	9.5 ± 0.7	0.18 ± 0.04
Pfu RPR + RPP21•RPP29 + POP5•RPP30	9.1 ± 0.6	0.18 ± 0.02

* The values reported are the mean and standard deviation from at least three independent trials. The curve-fit errors for k_{cat} and K_M were less than 25% in individual experiments. The experiment was performed essentially as described elsewhere (5). Assays were performed at 55°C in 50 mM Tris (pH 7.5), 0.8 M NH_4OAc and 30 mM $MgCl_2$. The *Pfu* RNase P holoenzyme was assembled using 10 nM folded RPR and 100 nM RPPs. The pre-tRNA^{Tyr} concentration range used for measuring the K_M was 31 - 2000 nM. Turnover numbers were calculated assuming that all of the RPR is assembled into holoenzyme.

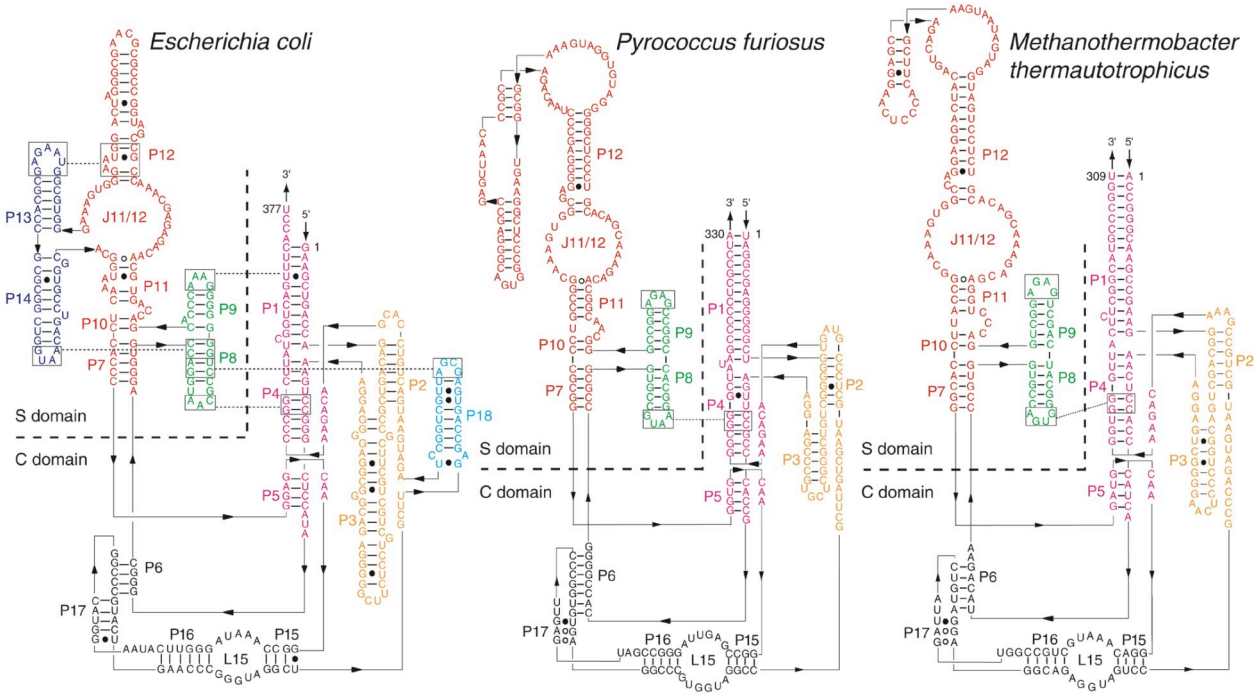

Figure S1. Secondary structures of *Eco*, *Pfu*, and *Mth* RPRs (13). Paired helices (e.g., P1, P2) are numbered consecutively from 5' to 3' and according to the *Eco* RPR nomenclature (13). A linker that joins helices P11 and P12 is termed J11/12. Boxes and dotted lines indicate loop-helix tertiary interactions.

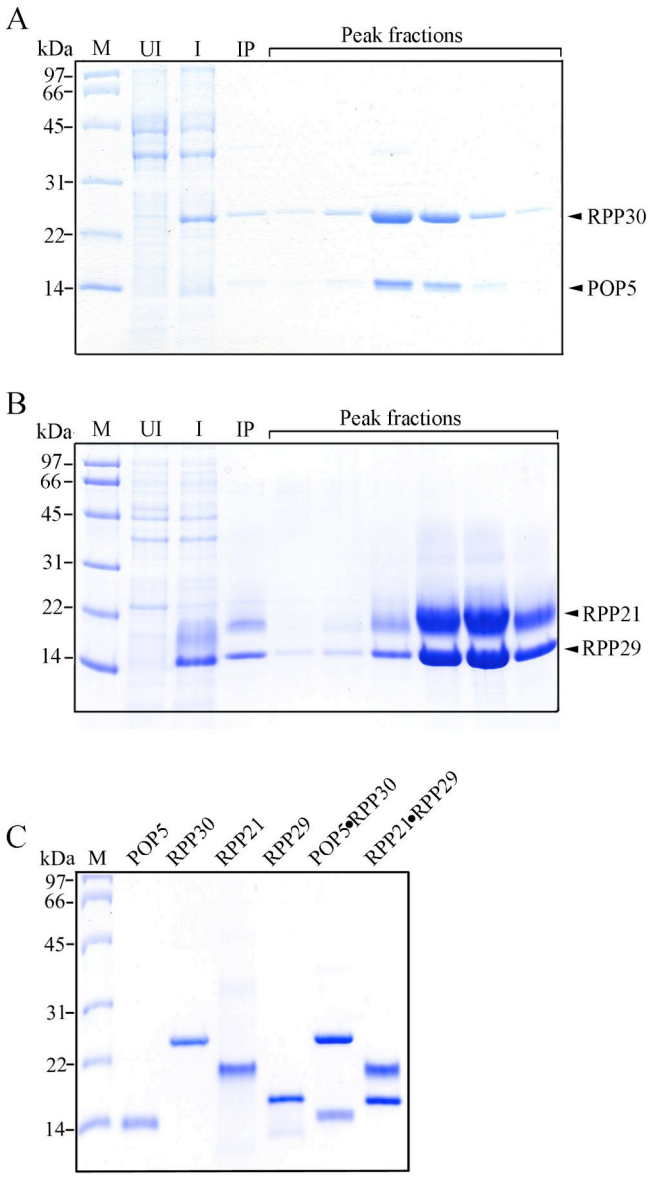

Figure S2. Purification of recombinant *Pfu* RPPs as binary complexes: (A) POP5•RPP30, (B) RPP21•RPP29 and (C) comparison of RPPs purified either individually or as binary complexes. M indicates size marker. UI and I denote the crude extracts from un-induced and induced cultures, respectively. IP represents the ammonium sulfate-fractionated sample that was subjected to the SP-sepharose column chromatography.

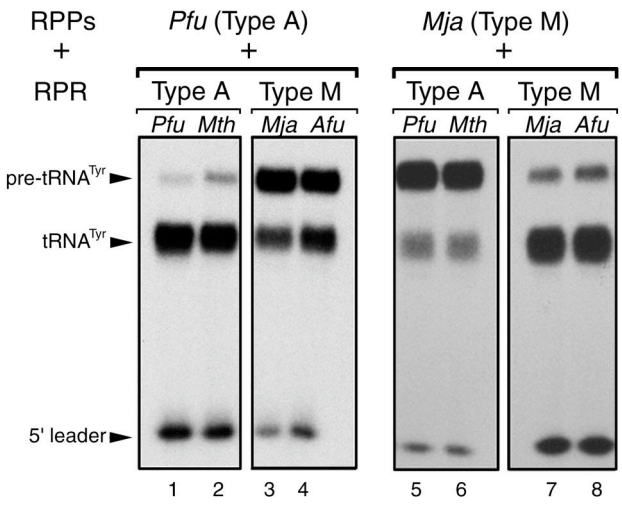

Figure S3. Heterologous reconstitution of RNase P holoenzymes using different archaeal RPRs and RPPs. Archaeal RPRs representing type A (*Pfu* and *Mth*) and M (*Mja* and *Afu*) were reconstituted with all four RPPs of either type A (*Pfu*) or M (*Mja*) RNase P. For these reconstitutions, 50 nM folded RPR was assembled with 250 nM RPPs in 50 mM Tris·HCl (pH 7.5), 800 mM NH_4OAc and 30 mM $Mg(OAc)_2$. The resulting RNPs were incubated with 500 nM pre-$tRNA^{Tyr}$ for 15 min at 55 °C.

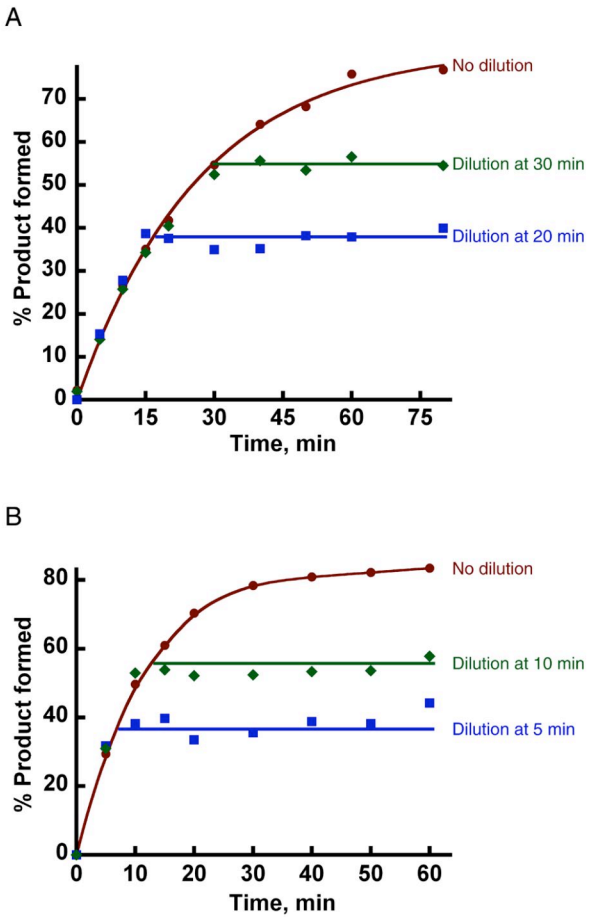

Figure S4. Pulse-chase experiments with *Mth* RNase P to demonstrate that the dissociation rate (k_{-1}) is greater than the rate of chemical cleavage (k_2) under single-turnover conditions. (A) *Mth* RPR (16.6 μM) and pre-tRNA^{Tyr} (2 nM) assayed in 50 mM MES (pH 5.8), 2 M NH_4OAc and 500 mM $MgCl_2$: the rate of chemical cleavage was measured without dilution (•) and after dilution at 20 min (■) or 30 min (◆). (B) *Mth* RPR + RPP21•RPP29 (3 μM) and pre-tRNA^{Tyr} (2 nM) assayed in 50 mM MES (pH 5.8), 800 mM NH_4OAc and 120 mM $MgCl_2$: the rate of chemical cleavage was measured without dilution (•) and after dilution at 5 min (■) or 10 min (◆). The green and blue lines indicate the plateau theoretically expected post-dilution when $k_{-1} >> k_2$.

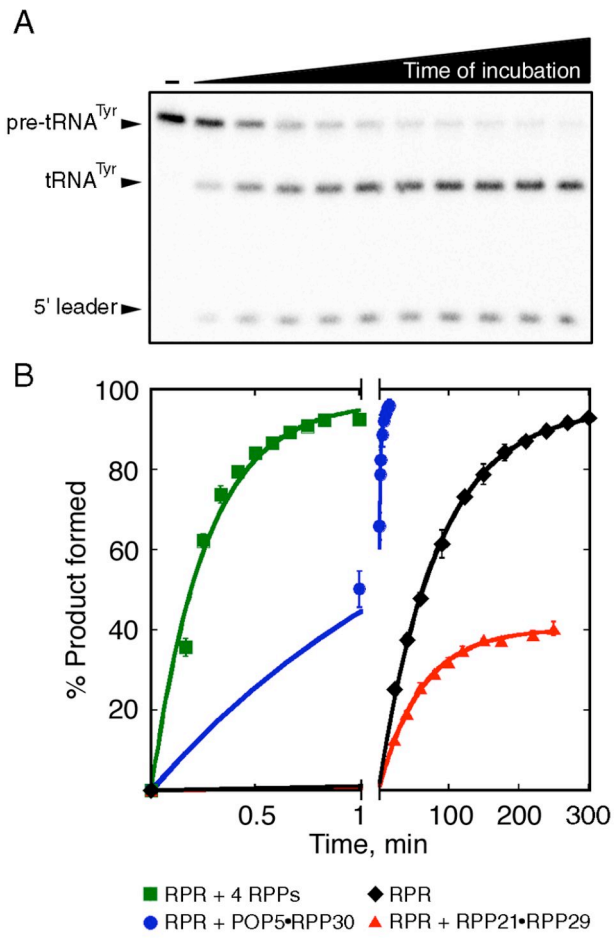

Figure S5. Effects of *Mth* RPPs on the single-turnover rate of *Mth* RPR-catalyzed pre-tRNA cleavage. (A) Increased product formation as a function of incubation time is illustrated in a representative time-course of pre-tRNA^{Tyr} processing by the *Mth* RNase P holoenzyme. (B) Examples of the curve fits of the rate of product formation by *Mth* RPR with and without RPPs under their respective optimal conditions (see Table I for details). The concentrations of *Mth* RPR, RPR + POP5•RPP30, RPR + RPP21•RPP29 and RPR + 4 RPPs used were 1.5 μM, 1.2 μM, 1.2 μM and 0.5 μM, respectively. Most of these ES complexes are productive as indicated by their ≥ 90% amplitudes, except for the reaction with RPR + RPP21•RPP29. Since we use a two-fold stoichiometric excess of RPPs:RPR to facilitate assembly of the respective RNP, it is possible that any RPP21•RPP29 uncomplexed with the RPR engages in RPR-independent

interactions with the pre-tRNA substrate and lowers the amplitude to 40%; however, this problem does not exist when RPP21•RPP29 is used in the context of 4 RPPs, presumably due to differences in assay conditions and/or the presence of POP5•RPP30.

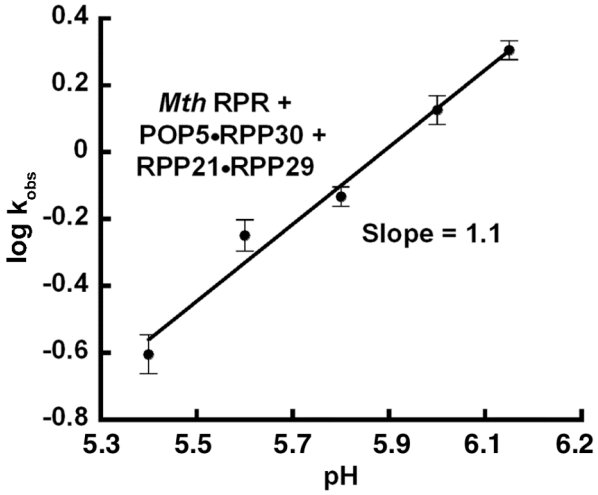

Figure S6. Dependence of k_{obs} on assay pH for *Mth* RPR + 4 RPPs. These single-turnover assays were performed with a vast excess of enzyme (3 μM) over the substrate (2 nM), and in 50 mM MES (indicated pH), 800 mM NH_4OAc and 20 mM $MgCl_2$. Note that the assays were performed in 20 mM Mg^{2+} and not 30 mM Mg^{2+}, which is optimal for the RPR + 4 RPPs; this change lowered the rate by ~6-fold and permitted manual rate measurements over the pH range used in this experiment.

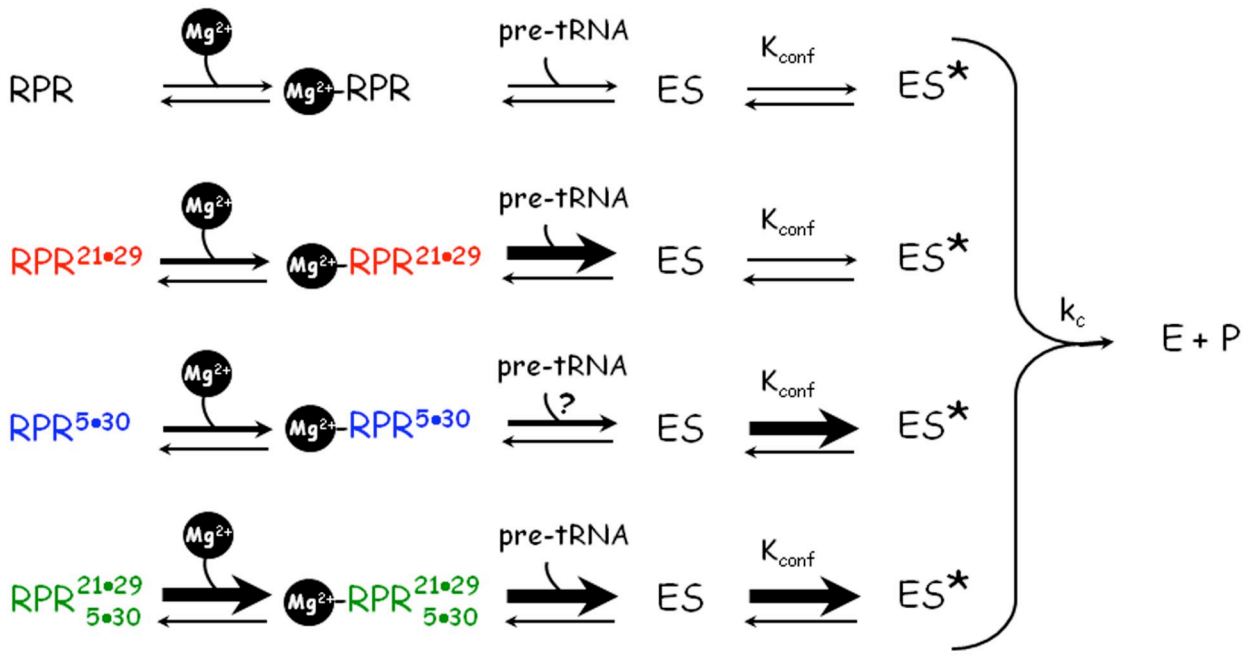

Figure S7. Kinetic scheme as a framework to interpret the contribution of the two binary RPP complexes to archaeal RNase P catalysis. For simplicity, the scheme does not take into account possible thermodynamic coupling in the binding of the RPPs (or pre-tRNA) and Mg^{2+} to the RPR. While the role of RPPs to binding of Mg^{2+} ions is indicated, no distinction is made between metal ions essential for RPR folding and catalysis. Although POP5•RPP30 reduced $K_{M(STO)}$ by two-fold in our single-turnover kinetic studies, in the absence of detailed binding studies, we are unable to comment on the role of this binary complex in substrate binding; this uncertainty is indicated by a question mark.